




 Cite this: *RSC Adv.*, 2022, 12, 34282

 Received 7th September 2022
 Accepted 21st November 2022

DOI: 10.1039/d2ra05655k

rsc.li/rsc-advances

A convenient catalytic method for preparation of new tetrahydropyrido[2,3-*d*]pyrimidines via a cooperative vinylogous anomeric based oxidation†

 Hassan Sepehrmansourie,^a Sima Kalhor,^a Mahmoud Zarei,^b ^{*b}
 Mohammad Ali Zolfigol ^{*a} and Mojtaba Hosseini^c

In this study, a novel functionalized metal–organic frameworks MIL-125(Ti)-N(CH₂PO₃H₂)₂ was designed and synthesized *via* post-modification methodology. Then, MIL-125(Ti)-N(CH₂PO₃H₂)₂ as a mesoporous catalyst was applied for the synthesis of a wide range of novel tetrahydropyrido[2,3-*d*]pyrimidines as bioactive candidate compounds by one-pot condensation reaction of 3-(1-methyl-1*H*-pyrrol-2-yl)-3-oxopropanenitrile, 6-amino-1,3-dimethylpyrimidine-2,4(1*H*,3*H*)-dione and aromatic aldehydes at 100 °C under solvent-free condition. Interestingly, the preparation of tetrahydropyrido[2,3-*d*]pyrimidine was achieved *via* vinylogous anomeric based oxidation mechanism with a high yield and short reaction time.

1 Introduction

Nowadays, metal–organic frameworks (MOFs) have been known as a unique type of porous solid materials, because they have been utilized in different fields such as drug delivery, catalyst, photocatalyst, battery, super capacitor, sensor, gas storage, separation and adsorption of molecules.^{1–3} These materials consist of multifunctional organic materials bound to metal or metal clusters through coordinated components such as carboxylates to form crystalline materials with high surface area and high thermal stability.^{4–8} Among them, the post-modification of metal–organic frameworks can be carried out with metal, acid and basic groups for preparation of biological molecules, which make motivational enzymes attractive for catalytic processes.^{9–11} Thus, post-modification improves the performance of the structure of metal–organic frameworks (MOFs) by applying changes in surface, pore size, thermal and chemical stability.^{12–14} The structure of titanium (Ti) based metal–organic frameworks is shown in Fig. 1.¹⁵ The research team developed post-modification of metal–organic frameworks based on Cr, Al and Zr,^{16–20} glycoluril,²¹ mesoporous materials (SBA-15),²² melamine,²³ and carbon quantum dots

(CQDs)²⁴ with phosphorus acid tags as a porous catalyst for the preparation of biological compounds.

Heterocyclic compounds containing N and/or O heteroatoms show biological properties.^{25,26} Therefore, the attention of many scientists has been attracted to the synthesis of these compounds. Amongst them, pyrido[2,3-*d*]pyrimidines are a well-known group of these compounds that show great importance of biological properties like adenosine kinase inhibitors, anti-tumor, antifungal, antibacterial, anti-proliferative CDK2 inhibitor, antipyretic, anticonvulsant agents, and analgesic while being used in CNS depressant activity (Fig. 2).^{27–31} The “anomeric effect” (AE) explains stereo-electronic interactions in the synthesis of molecules containing at least one heteroatom.³² The term cooperative anomeric effect has been introduced for electron sharing from two and/or more heteroatoms lone pairs to one acceptor antibonding orbital another atom. When anomeric effect developed *via* double bonds has been named “vinylogous anomeric effect”.

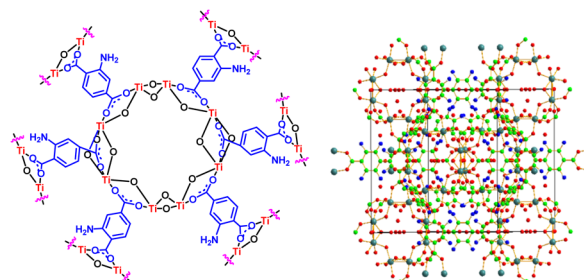


Fig. 1 Structure of titanium-based metal–organic frameworks MIL-125(Ti)-NH₂.

^aDepartment of Organic Chemistry, Faculty of Chemistry, Bu-Ali Sina University, Hamedan 6517838683, Iran. E-mail: mahmoud8103@yahoo.com; zolji@basu.ac.ir; mzolfigol@yahoo.com; Fax: +988138380709; Tel: +988138282807

^bDepartment of Chemistry, Faculty of Science, University of Qom, Qom, 37185-359, Iran. E-mail: mahmoud8103@yahoo.com

^cDepartment of Energy, Materials and Energy Research Center, P.O. Box 31787-316, Karaj, Iran. E-mail: m.hosseini@merc.ac.ir

† Electronic supplementary information (ESI) available. See DOI: <https://doi.org/10.1039/d2ra05655k>



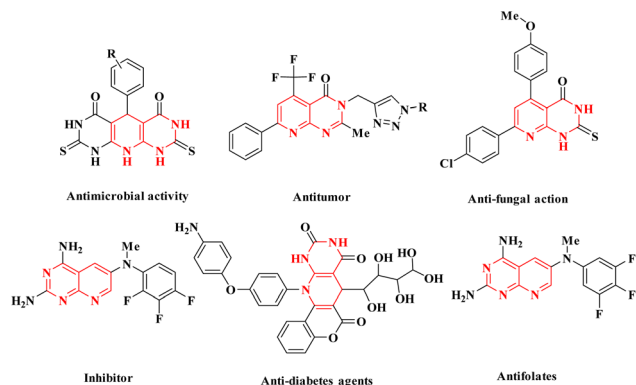


Fig. 2 Structure of pyrido[2,3-*d*]pyrimidines as a pharmacological candidate.

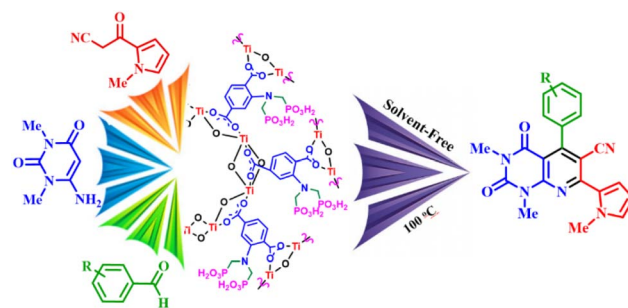
The “geminal anomeric effect” is compared with vinylogous anomeric effect (Fig. 3). In fact, the cooperative vinylogous anomeric effect is introduced for electron sharing *via* double bonds. Conversely, the geminal anomeric effect is introduced for electron donating and accepting from vicinal atoms.³³ Recently, we have introduced a new concept entitled “cooperative vinylogous anomeric based oxidation” for the synthesis of heterocycle compounds *via* a susceptible intermediate in the course of reaction.³⁴ In addition, this key phenomenon is observed in the oxidation/reduction mechanism and hydride transfer from NADPH/NADP⁺ and/or NADH/NAD⁺ systems.^{35–37}

Herein, based on the approach of post-modification, we have designed and synthesized novel MIL-125(Ti)-N(CH₂PO₃H₂)₂ as an efficient functionalized catalyst. This catalyst was tested for the preparation of novel tetrahydropyrido[2,3-*d*]pyrimidines by one-pot condensation reaction of aldehydes, 6-amino-1,3-dimethylpyrimidine-2,4(1*H*,3*H*)-dione and 3-(1-methyl-1*H*-pyrrol-2-yl)-3-oxopropanenitrile *via* a cooperative vinylogous anomeric based oxidation mechanism (Scheme 1).

2 Experimental

2.1 Materials and methods

All materials and solvents such as 2-amino terephthalic acid (NH₂-H₂BDC) (Merck, 95%), DMF (Merck, 99%), titanium tetraisopropanolate (TTIP) (Aldrich, 99.8%), methanol (Merck, 96%), ethanol (Merck, 99%), paraformaldehyde, phosphorous acid, *p*-toluene sulfonic acid (*p*-TSA), 6-amino-1,3-



Scheme 1 Synthesis of novel tetrahydropyrido[2,3-*d*]pyrimidines using MIL-125(Ti)-N(CH₂PO₃H₂)₂ as a porous catalyst.

dimethylpyrimidine-2,4(1*H*,3*H*)-dione-1-methyl-1*H*-pyrrole (Merck, 96%), 2-cyanoacetic acid were purchased and used without further purification.

2.2 Instrumental techniques

The (FT-IR) technique model device, (PerkinElmer Spectrum Version 10.02.00) was used to identify the functional groups. The morphology and microstructure of the different stages of synthesized catalyst were characterized using a SEM technique (TESCAN MIRA-II (Czechia)). EDS was carried out by the model (TESCAN MIRA-II (Czechia)). The thermal stability of the prepared porous catalyst was determined by a thermogravimetric analyzer/derivative thermogravimetry (TGA/DTG, TGA2, Mettler Toledo) at a heating rate of 10 °C min⁻¹ under N₂ atmosphere. BET technique with model device (BELSORP-mini-II) was used to determine the surface area and pore size of different stages of the synthesized catalyst and XRD patterns of the different stages synthesized catalyst were detected by X-ray diffractometer (PHILIPS PW1730 (Netherlands)).

2.3 General procedure for the preparation of MIL-125(Ti)-N(CH₂PO₃H₂)₂

Firstly, MIL-125(Ti)-NH₂ was synthesized according to the literature survey.³⁸ In the following, a mixture of MIL-125(Ti)-NH₂, (0.5 g), paraformaldehyde (3 mmol, 0.09 g), phosphorous acid (2 mmol, 0.164 g) and *p*-TSA (0.02 g) was refluxed in EtOH (50 mL) as a solvent for 12 h. After this time, the obtained solid was filtered by centrifugation (1000 rpm, 10 min), and washed with EtOH (2 × 10 mL) at room temperature. The precipitate was dried under vacuum oven at 80 °C for 12 h to give MIL-125(Ti)-N(CH₂PO₃H₂)₂ (Scheme 2).

2.4 General procedure for the synthesis of novel tetrahydropyrido[2,3-*d*]pyrimidines using MIL-125(Ti)-N(CH₂PO₃H₂)₂ as a porous catalyst

Initially, 3-(1-methyl-1*H*-pyrrol-2-yl)-3-oxopropanenitrile was prepared according to the literature survey (Scheme 3).³⁹ Then, in a 25 mL round-bottomed flask a mixture of aryl aldehydes (1 mmol), 6-amino-1,3-dimethylpyrimidine-2,4(1*H*,3*H*)-dione (1 mmol, 0.155 g), 3-(1-methyl-1*H*-pyrrol-2-yl)-3-oxopropanenitrile (1 mmol, 0.148 g) and MIL-125(Ti)-N(CH₂PO₃H₂)₂ (10 mg) as

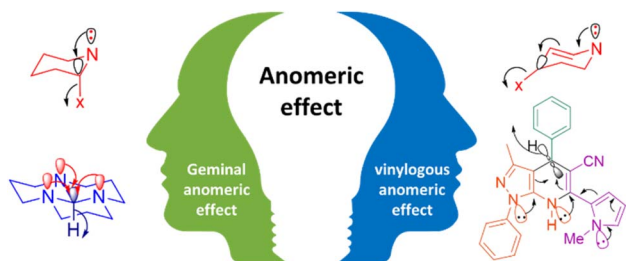
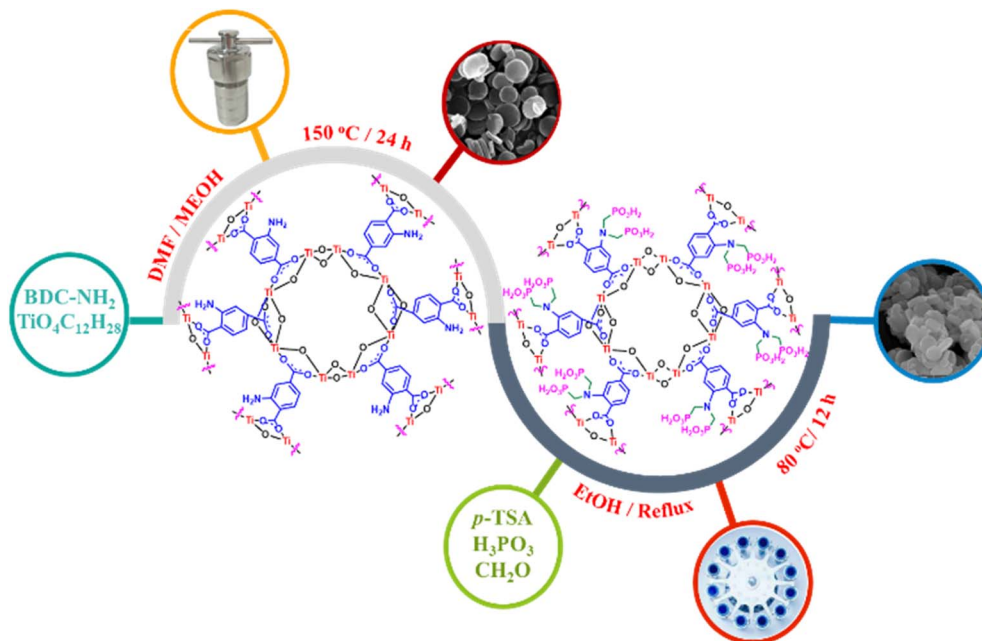


Fig. 3 Comparison of geminal and vinylogous anomeric effect.



Scheme 2 Synthesis of MIL-125(Ti)-NH₂ and MIL-125(Ti)-N(CH₂PO₃H₂)₂.

a porous catalyst was stirred at 100 °C under solvent-free condition. After the completion of the reactions which were monitored by the TLC technique (*n*-hexane : ethyl acetate; 7 : 3). Then, the described catalyst was separated from the reaction mixture by centrifugation (1000 rpm) after adding hot EtOH (20 mL) as a solvent. Finally, after the evaporation of the solvent at room temperature, the pure product was obtained by washing with hot ethanol and water (Scheme 3).

2.5 Spectral data

2.5.1 5-(4-Chlorophenyl)-1,3-dimethyl-7-(1-methyl-1*H*-pyrrol-2-yl)-2,4-dioxo-1,2,3,4-tetrahydropyrido[2,3-*d*]pyrimidine-6-carbonitrile (A1). Yellow solid; mp: 248–250 °C; FT-IR (KBr, cm⁻¹): 3113, 2998, 2949, 2219, 1709, 1663. ¹H NMR (400 MHz, DMSO-*d*₆) δ_{ppm} 7.56 (d, *J* = 8.5 Hz, 2H), 7.37 (d, *J* = 8.5 Hz, 2H), 7.25 (t, *J* = 1.6 Hz, 1H), 7.20 (dd, *J* = 4.1, 1.6 Hz, 1H), 6.26 (dd, *J* = 4.1, 2.5 Hz, 1H), 4.01 (s, 3H), 3.65 (s, 3H), 3.16 (s, 3H).

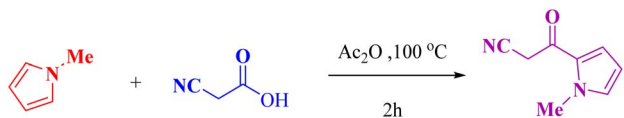
2.5.2 1,3-Dimethyl-7-(1-methyl-1*H*-pyrrol-2-yl)-2,4-dioxo-5-(*p*-tolyl)-1,2,3,4-tetrahydropyrido[2,3-*d*]pyrimidine-6-carbonitrile (A2). Yellow solid; mp: 228–230 °C; FT-IR (KBr, cm⁻¹): 3123, 2960, 2873, 2220, 1717, 1674. ¹H NMR (400 MHz, DMSO-*d*₆) δ_{ppm} 7.39 (d, *J* = 7.9 Hz, 2H), 7.34 (t, *J* = 1.6 Hz, 1H), 7.32 (s, 1H), 7.31–7.28 (m, 2H), 6.36 (dd, *J* = 4.0, 2.6 Hz, 1H), 4.11 (s, 3H), 3.75 (s, 3H), 3.26 (s, 3H), 2.52 (s, 3H). ¹³C NMR

(101 MHz, DMSO-*d*₆) δ_{ppm} 158.8, 158.54, 154.4, 151.8, 150.6, 137.7, 133.7, 130.7, 128.4, 127.4, 127.2, 117.2, 117.0, 108.2, 104.9, 101.6, 37.30, 30.32, 28.11, 20.95.

2.5.3 5-(4-Methoxyphenyl)-1,3-dimethyl-7-(1-methyl-1*H*-pyrrol-2-yl)-2,4-dioxo-1,2,3,4-tetrahydropyrido[2,3-*d*]pyrimidine-6-carbonitrile (A3). Yellow solid; mp: 230–233 °C; FT-IR (KBr, cm⁻¹): 3369, 3142, 2981, 2219, 1709, 1662. ¹H NMR (400 MHz, DMSO-*d*₆) δ_{ppm} 7.27 (d, *J* = 8.7 Hz, 2H), 7.24 (t, *J* = 1.6 Hz, 1H), 7.19 (dd, *J* = 4.0, 1.6 Hz, 1H), 7.03 (d, *J* = 8.7 Hz, 2H), 6.25 (dd, *J* = 4.0, 2.6 Hz, 1H), 4.01 (s, 3H), 3.85 (s, 3H), 3.65 (s, 3H), 3.17 (s, 3H). ¹³C NMR (101 MHz, DMSO-*d*₆) δ_{ppm} 159.4, 158.6, 158.6, 154.4, 151.9, 150.6, 130.7, 129.2, 128.5, 127.2, 117.2, 117.2, 113.2, 108.2, 104.9, 101.8, 55.0, 37.3, 30.3, 28.1.

2.5.4 1,3-Dimethyl-7-(1-methyl-1*H*-pyrrol-2-yl)-2,4-dioxo-5-phenyl-1,2,3,4-tetrahydropyrido[2,3-*d*]pyrimidine-6-carbonitrile (A4). Yellow solid; mp: 228–230 °C; FT-IR (KBr, cm⁻¹): 3116, 2951, 2213, 1714, 1670. ¹H NMR (400 MHz, DMSO-*d*₆) δ_{ppm} 7.50–7.46 (m, 3H), 7.32 (dd, *J* = 6.6, 2.9 Hz, 2H), 7.24 (t, *J* = 1.6 Hz, 1H), 7.19 (dd, *J* = 4.1, 1.6 Hz, 1H), 6.26 (dd, *J* = 4.0, 2.6 Hz, 1H), 4.02 (s, 3H), 3.66 (s, 3H), 3.16 (s, 3H). ¹³C NMR (101 MHz, DMSO-*d*₆) δ_{ppm} 158.6, 158.5, 154.4, 151.8, 150.7, 136.7, 130.8, 128.4, 127.8, 127.4, 127.2, 117.2, 116.9, 108.3, 104.8, 101.5, 37.3, 30.3, 28.1.

2.5.5 1,3-Dimethyl-7-(1-methyl-1*H*-pyrrol-2-yl)-2,4-dioxo-5-(*m*-tolyl)-1,2,3,4-tetrahydropyrido[2,3-*d*]pyrimidine-6-carbonitrile (A5). Yellow solid; mp: 180–182 °C; FT-IR (KBr, cm⁻¹): 3118, 2920, 2219, 1714, 1668. ¹H NMR (400 MHz, DMSO-*d*₆) δ_{ppm} 7.37 (t, *J* = 7.6 Hz, 1H), 7.28 (d, *J* = 7.7 Hz, 1H), 7.24 (t, *J* = 1.9 Hz, 1H), 7.19 (dd, *J* = 4.1, 1.7 Hz, 1H), 7.13–7.08 (m, 2H), 6.25 (dd, *J* = 4.1, 2.5 Hz, 1H), 4.01 (s, 3H), 3.65 (s, 3H), 3.16 (s, 3H), 2.37 (s, 3H). ¹³C NMR (101 MHz, DMSO-*d*₆) δ_{ppm} 158.8, 158.4, 154.3, 151.8, 150.7, 136.8, 136.7, 130.7, 129.0,



Scheme 3 Preparation of 3-(1-methyl-1*H*-pyrrol-2-yl)-3-oxopropanenitrile.

127.8, 127.6, 127.2, 124.5, 117.2, 116.9, 108.3, 104.8, 101.5, 37.3, 30.3, 28.1, 21.0.

2.5.6 5-(4-Fluorophenyl)-1,3-dimethyl-7-(1-methyl-1H-pyrrol-2-yl)-2,4-dioxo-1,2,3,4-tetrahydropyrido[2,3-d]pyrimidine-6-carbonitrile (A6). Yellow solid; mp: 289–290 °C; FT-IR (KBr, cm^{-1}): 3119, 2955, 2213, 1716, 1662. ^1H NMR (400 MHz, $\text{DMSO}-d_6$) δ_{ppm} 7.41–7.37 (m, 2H), 7.35–7.30 (m, 2H), 7.25 (t, $J = 1.7$ Hz, 1H), 7.20 (dd, $J = 4.1, 1.7$ Hz, 1H), 6.26 (dd, $J = 4.1, 2.5$ Hz, 1H), 4.01 (s, 3H), 3.66 (s, 3H), 3.17 (s, 3H). ^{13}C NMR (101 MHz, $\text{DMSO}-d_6$) δ_{ppm} 163.4, 161.0, 158.6, 157.7, 154.3, 151.8, 150.6, 133.0, 130.9, 129.9, 127.2, 117.3, 117.0, 115.0, 114.8, 108.3, 105.0, 101.6, 37.3, 30.3, 28.1.

2.5.7 5-(4-Hydroxyphenyl)-1,3-dimethyl-7-(1-methyl-1H-pyrrol-2-yl)-2,4-dioxo-1,2,3,4-tetrahydropyrido[2,3-d]pyrimidine-6-carbonitrile (A7). Yellow solid; mp: >300 °C; FT-IR (KBr, cm^{-1}): 3306, 3080, 2942, 2223, 1727, 1653. ^1H NMR (400 MHz, $\text{DMSO}-d_6$) δ_{ppm} 9.72 (s, 1H), 7.23 (t, $J = 1.6$ Hz, 1H), 7.18 (dd, $J = 4.1, 1.7$ Hz, 1H), 7.14 (d, $J = 8.6$ Hz, 2H), 6.84 (d, $J = 8.6$ Hz, 2H), 6.25 (dd, $J = 4.0, 2.6$ Hz, 1H), 4.00 (s, 3H), 3.64 (s, 3H), 3.17 (s, 3H). ^{13}C NMR (101 MHz, $\text{DMSO}-d_6$) δ_{ppm} 159.1, 158.5, 157.8, 154.4, 151.9, 150.7, 130.6, 129.2, 127.3, 126.8, 117.3, 117.2, 114.6, 108.2, 104.9, 101.9, 37.2, 30.3, 28.

2.5.8 5-(2-Methoxyphenyl)-1,3-dimethyl-7-(1-methyl-1H-pyrrol-2-yl)-2,4-dioxo-1,2,3,4-tetrahydropyrido[2,3-d]pyrimidine-6-carbonitrile (A8). Yellow solid; mp: 205–208 °C; FT-IR (KBr, cm^{-1}): 3447, 2219, 1718, 1665. ^1H NMR (400 MHz, $\text{DMSO}-d_6$) δ_{ppm} 7.24–7.14 (t, $J = 7.1$ Hz, 1H), 7.18 (m, 4H), 7.10–7.03 (m, 1H), 6.25 (s, 1H), 4.02 (s, 3H), 3.73 (s, 3H), 3.65 (s, 3H), 3.17 (s, 3H). ^{13}C NMR (101 MHz, $\text{DMSO}-d_6$) δ_{ppm} 158.3, 156.3, 155.5, 154.4, 151.8, 150.6, 130.8, 130.2, 128.5, 127.2, 125.5, 120.3, 117.1, 116.9, 111.1, 108.3, 105.3, 101.7, 55.5, 37.4, 30.3, 28.0.

2.5.9 5-(4-Bromophenyl)-1,3-dimethyl-7-(1-methyl-1H-pyrrol-2-yl)-2,4-dioxo-1,2,3,4-tetrahydropyrido[2,3-d]pyrimidine-6-carbonitrile (A9). Yellow solid; mp: 266–268 °C; FT-IR (KBr, cm^{-1}): 3116, 2952, 2221, 1715, 1669. ^1H NMR (400 MHz, $\text{DMSO}-d_6$) δ_{ppm} 7.70 (d, $J = 8.4$ Hz, 2H), 7.30 (d, $J = 8.5$ Hz, 2H), 7.25 (t, $J = 1.7$ Hz, 1H), 7.20 (dd, $J = 4.1, 1.7$ Hz, 1H), 6.26 (dd, $J = 4.1, 2.5$ Hz, 1H), 4.01 (s, 3H), 3.65 (s, 3H), 3.16 (s, 3H). ^{13}C NMR (101 MHz, $\text{DMSO}-d_6$) δ_{ppm} 158.6, 157.3, 154.4, 151.8, 150.6, 136.0, 130.9, 130.9, 129.7, 127.2, 122.0, 117.3, 116.9, 108.4, 104.7, 101.2, 37.3, 30.3, 28.1.

2.5.10 1,3-Dimethyl-7-(1-methyl-1H-pyrrol-2-yl)-5-(4-nitrophenyl)-2,4-dioxo-1,2,3,4-tetrahydropyrido[2,3-d]pyrimidine-6-carbonitrile (A10). Yellow solid; mp: 233–235 °C; FT-IR (KBr, cm^{-1}): 3427, 2948, 2219, 1712, 1664. ^1H NMR (400 MHz, $\text{DMSO}-d_6$) δ_{ppm} 8.37 (d, $J = 8.8$ Hz, 2H), 7.66 (d, $J = 8.8$ Hz, 2H), 7.27 (t, $J = 1.6$ Hz, 1H), 7.22 (dd, $J = 4.1, 1.6$ Hz, 1H), 6.27 (dd, $J = 4.1, 2.5$ Hz, 1H), 4.03 (s, 3H), 3.67 (s, 3H), 3.16 (s, 3H). ^{13}C NMR (101 MHz, $\text{DMSO}-d_6$) δ_{ppm} 158.7, 156.3, 154.4, 151.8, 150.6, 147.4, 143.9, 131.2, 129.1, 127.1, 123.2, 117.5, 116.7, 108.5, 104.6, 100.6, 37.4, 30.3, 28.1.

2.5.11 5-(2,4-Dichlorophenyl)-1,3-dimethyl-7-(1-methyl-1H-pyrrol-2-yl)-2,4-dioxo-1,2,3,4-tetrahydropyrido[2,3-d]pyrimidine-6-carbonitrile (A11). Yellow solid; mp: 210–213 °C; FT-IR (KBr, cm^{-1}): 3109, 2942, 2219, 1722, 1659. ^1H NMR (400 MHz, $\text{DMSO}-d_6$) δ_{ppm} 7.83 (d, $J = 2.0$ Hz, 1H), 7.60 (dd, $J = 8.3,$

2.0 Hz, 1H), 7.40 (d, $J = 8.3$ Hz, 1H), 7.28 (t, $J = 1.7$ Hz, 1H), 7.24 (dd, $J = 4.1, 1.7$ Hz, 1H), 6.28 (dd, $J = 4.1, 2.5$ Hz, 1H), 4.04 (s, 3H), 3.66 (s, 3H), 3.18 (s, 3H). ^{13}C NMR (101 MHz, $\text{DMSO}-d_6$) δ_{ppm} 158.4, 154.5, 154.5, 151.9, 150.5, 134.9, 134.1, 131.7, 131.4, 130.4, 128.6, 127.5, 127.0, 117.5, 116.4, 108.6, 104.8, 100.6, 37.5, 30.3, 28.1.

2.5.12 5-(3-Hydroxyphenyl)-1,3-dimethyl-7-(1-methyl-1H-pyrrol-2-yl)-2,4-dioxo-1,2,3,4-tetrahydropyrido[2,3-d]pyrimidine-6-carbonitrile (A12). Yellow solid; mp: 156–158 °C; FT-IR (KBr, cm^{-1}): 3116, 2945, 2216, 1714, 1667. ^1H NMR (400 MHz, $\text{DMSO}-d_6$) δ_{ppm} 9.58 (s, 1H), 7.26 (dd, $J = 13.4, 5.2$ Hz, 2H), 7.18 (dd, $J = 4.1, 1.6$ Hz, 1H), 6.85 (dd, $J = 8.1, 1.7$ Hz, 1H), 6.71–6.66 (m, 2H), 6.25 (dd, $J = 4.0, 2.5$ Hz, 1H), 4.01 (s, 3H), 3.65 (s, 3H), 3.17 (s, 3H). ^{13}C NMR (101 MHz, $\text{DMSO}-d_6$) δ_{ppm} 158.6, 158.3, 156.8, 154.3, 151.8, 150.7, 137.9, 130.7, 129.1, 127.2, 117.9, 117.2, 116.9, 115.3, 114.2, 108.3, 104.8, 101.4, 37.3, 30.3, 28.1.

2.5.13 5-(2-Chlorophenyl)-1,3-dimethyl-7-(1-methyl-1H-pyrrol-2-yl)-2,4-dioxo-1,2,3,4-tetrahydropyrido[2,3-d]pyrimidine-6-carbonitrile (A13). Yellow solid; mp: >300 °C; FT-IR (KBr, cm^{-1}): 3113, 2949, 2998, 2219, 1709, 1663. ^1H NMR (400 MHz, $\text{DMSO}-d_6$) δ_{ppm} 7.63–7.60 (m, 1H), 7.54–7.45 (m, 2H), 7.34 (dd, $J = 7.4, 1.8$ Hz, 1H), 7.28 (t, $J = 1.6$ Hz, 1H), 7.22 (dd, $J = 4.1, 1.6$ Hz, 1H), 6.28 (dd, $J = 4.1, 2.5$ Hz, 1H), 4.04 (s, 3H), 3.67 (s, 3H), 3.17 (s, 3H). ^{13}C NMR (101 MHz, $\text{DMSO}-d_6$) δ_{ppm} 158.3, 155.6, 154.5, 151.9, 150.5, 135.8, 131.2, 130.4, 130.2, 129.0, 128.9, 127.2, 127.0, 117.4, 116.4, 108.54, 37.5, 30.3, 28.1.

2.5.14 5-(4-Isopropylphenyl)-1,3-dimethyl-7-(1-methyl-1H-pyrrol-2-yl)-2,4-dioxo-1,2,3,4-tetrahydropyrido[2,3-d]pyrimidine-6-carbonitrile (A14). Yellow solid; mp: 190–192 °C; FT-IR (KBr, cm^{-1}): 3110, 2955, 2853, 2219, 1712, 1663. ^1H NMR (400 MHz, $\text{DMSO}-d_6$) δ_{ppm} 7.35 (d, $J = 8.1$ Hz, 2H), 7.27–7.23 (m, $J = 8.0$ Hz, 3H), 7.18 (dd, $J = 4.1, 1.6$ Hz, 1H), 6.25 (dd, $J = 4.0, 2.6$ Hz, 1H), 4.01 (s, 3H), 3.65 (s, 3H), 3.16 (s, 3H), 2.99 (hep, $J = 6.9$ Hz, 1H), 1.29 (d, $J = 6.9$ Hz, 6H). ^{13}C NMR (101 MHz, $\text{DMSO}-d_6$) δ_{ppm} 158.8, 158.5, 154.4, 151.9, 150.7, 148.4, 134.0, 130.7, 127.5, 127.2, 125.7, 117.2, 117.0, 108.3, 104.9, 101.6, 37.2, 33.1, 30.3, 28.1, 23.7.

2.5.15 5-(3-Ethoxy-4-hydroxyphenyl)-1,3-dimethyl-7-(1-methyl-1H-pyrrol-2-yl)-2,4-dioxo-1,2,3,4-tetrahydropyrido[2,3-d]pyrimidine-6-carbonitrile (A15). Yellow solid; mp: 246–248 °C; FT-IR (KBr, cm^{-1}): 3106, 3060, 2942, 2218, 1715, 1670. ^1H NMR (400 MHz, $\text{DMSO}-d_6$) δ_{ppm} 9.21 (s, 1H), 7.23 (t, $J = 1.9$ Hz, 1H), 7.18 (dd, $J = 4.0, 1.6$ Hz, 1H), 6.93–6.85 (m, 2H), 6.74 (dd, $J = 8.1, 1.9$ Hz, 1H), 6.25 (dd, $J = 4.0, 2.6$ Hz, 1H), 4.04–3.98 (m, 5H), 3.64 (s, 3H), 3.17 (s, 3H), 1.33 (t, $J = 6.9$ Hz, 3H). ^{13}C NMR (101 MHz, $\text{DMSO}-d_6$) δ_{ppm} 158.9, 158.5, 154.3, 151.8, 150.7, 147.3, 145.9, 130.6, 127.3, 127.2, 120.7, 117.3, 117.2, 115.0, 113.7, 108.2, 105.0, 101.9, 63.8, 37.2, 30.3, 28.1, 14.5.

2.5.16 1,3-Dimethyl-7-(1-methyl-1H-pyrrol-2-yl)-5-(naphthalen-1-yl)-2,4-dioxo-1,2,3,4-tetrahydropyrido[2,3-d]pyrimidine-6-carbonitrile (A16). Yellow solid; mp: 212–214 °C; FT-IR (KBr, cm^{-1}): 3113, 2945, 2219, 1709, 1663. ^1H NMR (400 MHz, $\text{DMSO}-d_6$) δ_{ppm} 8.04 (d, $J = 8.3$ Hz, 2H), 7.65–7.60 (m, 1H), 7.57–7.53 (m, 1H), 7.43 (d, $J = 3.8$ Hz, 2H), 7.39 (dd, $J = 7.0, 0.7$ Hz, 1H), 7.26 (t, $J = 1.6$ Hz, 1H), 7.18 (dd, $J = 4.1, 1.6$ Hz, 1H), 6.25 (dd, $J = 4.1, 2.5$ Hz, 1H), 4.07 (s, 3H), 3.71 (s, 3H), 3.07 (s,

3H). ^{13}C NMR (101 MHz, $\text{DMSO-}d_6$) δ_{ppm} 158.4, 150.7, 136.8, 134.2, 130.7, 128.6, 127.7, 127.2, 126.2, 118.6, 117.2, 108.9, 108.3, 104.9, 37.2, 30.3, 28.1.

2.5.17 5,5'-(1,4-Phenylene)bis(1,3-dimethyl-7-(1-methyl-1H-pyrrol-2-yl)-2,4-dioxo-1,2,3,4-tetrahydropyrido[2,3-d]pyrimidine-6-carbonitrile) (A17). Yellow solid; mp: >300 °C; FT-IR (KBr, cm^{-1}): 2951, 2928, 2216, 1716, 1667. ^1H NMR (400 MHz, $\text{DMSO-}d_6$) δ_{ppm} 7.46 (s, 4H), 7.26–7.23 (m, $J = 3.7$ Hz, 4H), 6.28–6.25 (m, 2H), 4.03 (s, 6H), 3.68 (s, 6H), 3.23 (s, 3H), 3.18 (s, 3H). ^{13}C NMR (101 MHz, $\text{DMSO-}d_6$) δ_{ppm} 155.1, 154.9, 153.1, 152.2, 151.4, 150.9, 143.5, 131.8, 131.7, 131.3, 131.0, 128.2, 127.2, 117.9, 117.6, 116.9, 115.9, 108.7, 108.4, 107.8, 106.5, 104.3, 99.7, 98.6, 37.8, 37.4, 30.4, 29.7, 28.1.

3 Results and discussion

Development of “anomeric based oxidation” concept, from synthesis of heterocycle compounds *via* a susceptible intermediate in the course of reaction is our main research demand because this key phenomenon is observed in the oxidation/reduction mechanism and hydride transfer from NADPH/NADP⁺ and/or NADH/NAD⁺ biological systems.^{35–37} With this aim, the described porous metal–organic framework containing phosphorous acid groups MIL-125(Ti)-N(CH₂PO₃H₂)₂ as a porous catalyst was synthesized and applied for the preparation of tetrahydropyrido[2,3-d]pyrimidines *via* a cooperative vinylogous anomeric based oxidation mechanism. To shed light on more details, the structure of MIL-125(Ti)-N(CH₂PO₃H₂)₂ as a porous material catalyst was thoroughly approved by various analyses; FT-IR, X-ray diffraction analysis (XRD), energy-dispersive X-ray spectroscopy (EDX), scanning electron microscope (SEM), N₂ absorption and desorption, thermal gravimetric (TGA) and derivative thermogravimetry (DTG).

FT-IR analysis of MIL-125(Ti)-NH₂ and MIL-125(Ti)-N(CH₂PO₃H₂)₂ were compared in Fig. 4. The bands at 3384 and 3462 cm^{-1} indicates the symmetric and asymmetric vibrations of the NH₂ groups in MIL-125(Ti)-NH₂. The broad peak at 2800–3600 cm^{-1} is related to the OH of PO₃H₂ functional groups in

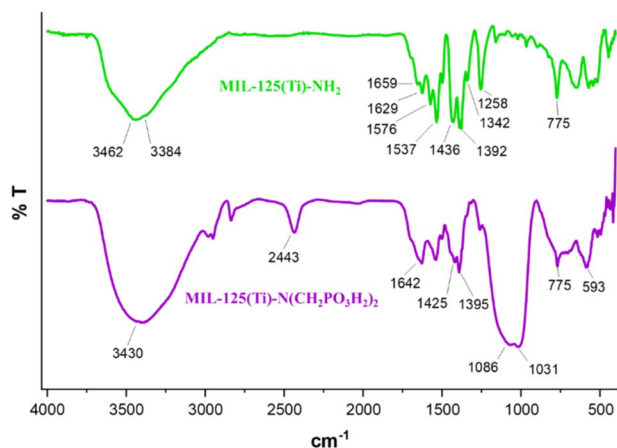


Fig. 4 FT-IR spectra of MIL-125(Ti)-NH₂ and MIL-125(Ti)-N(CH₂PO₃H₂)₂ as a porous catalyst.

MIL-125(Ti)-N(CH₂PO₃H₂)₂. The absorption bands at 1659 cm^{-1} in MIL-125(Ti)-NH₂ are assigned to C=O bond stretching of carboxylic acid group. Also, the absorption bands at 1031 and 1086 cm^{-1} are assigned to P–O bond stretching. Furthermore, the absorption band at 775 cm^{-1} is related to Ti metal. The changes between the FT-IR spectrums of MIL-125(Ti)-NH₂ and MIL-125(Ti)-N(CH₂PO₃H₂)₂ verified the successful post-modification.

The XRD patterns of MIL-125(Ti)-NH₂ and MIL-125(Ti)-N(CH₂PO₃H₂)₂ were described in Fig. 5. As shown in Fig. 5, the pattern of peak of MIL-125(Ti)-NH₂ is similar to the literature references.^{40–42} Also, the XRD results of post-modification with phosphorous acid groups is almost unchanged with MIL-125(Ti)-NH₂. According to the XRD profile, the morphology and structure of the catalyst remained constant at different stages of synthesis.

The crystal scaffolds of MIL-125(Ti)-NH₂ and MIL-125(Ti)-N(CH₂PO₃H₂)₂ were checked out by energy dispersive X-ray analysis (EDX) (Fig. 6). According to the EDX analysis approved the existence elements structure of C, N, and Ti in MIL-125(Ti)-NH₂ and P, O, N, and Ti in MIL-125(Ti)-N(CH₂PO₃H₂)₂ respectively.

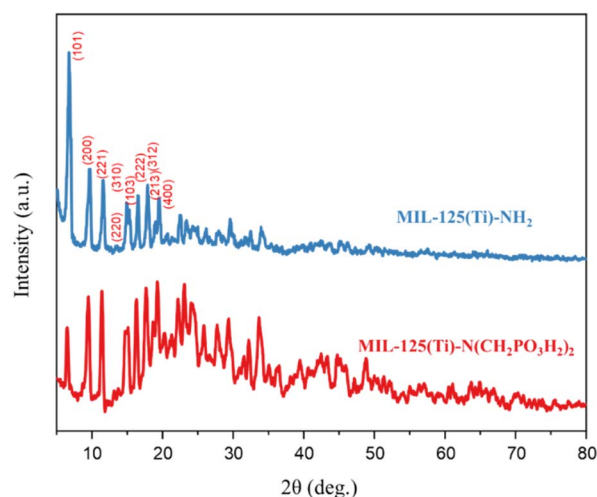


Fig. 5 XRD patterns of MIL-125(Ti)-NH₂ and MIL-125(Ti)-N(CH₂PO₃H₂)₂ as a porous catalyst.

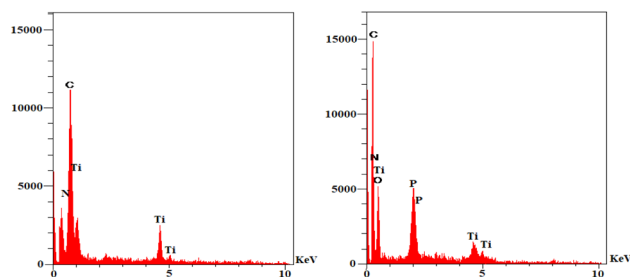


Fig. 6 EDX analysis of MIL-125(Ti)-NH₂ and MIL-125(Ti)-N(CH₂PO₃H₂)₂ as a porous catalyst.

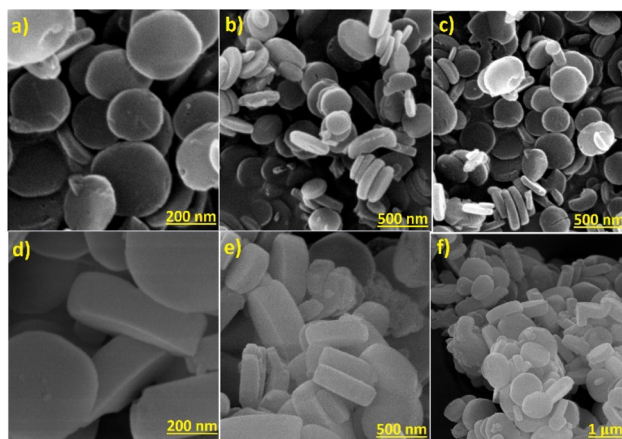


Fig. 7 SEM images of MIL-125(Ti)-NH₂ (a–c) and MIL-125(Ti)-N(CH₂PO₃H₂)₂ (d–f) as a porous catalyst.

In another study, the morphology of MIL-125(Ti)-NH₂ and its post-modification were investigated by scanning electron microscope (SEM) (Fig. 7). As shown in Fig. 7a–c, the uniform tablet-like form and smooth surface shape of MIL-125(Ti)-NH₂ exhibit, which is similar to the literature reference.⁴⁰ Also, the morphology of MIL-125(Ti)-NH₂ after post-modification with phosphorus acid tags is unchanged and stable (Fig. 7d–f). As shown, the obtained XRD pattern confirmed the resulting image from SEM analysis.

The textural properties of MIL-125(Ti)-NH₂ and MIL-125(Ti)-N(CH₂PO₃H₂)₂ were studied by N₂ adsorption–desorption isotherms (Fig. 8a). The absence of the hysteresis loop indicates the absence of mesoporous in the samples. The calculated surface areas based on the BET equation are 1328 and 554 m² g^{−1} for MIL-125(Ti)-NH₂ and MIL-125(Ti)-N(CH₂PO₃H₂)₂ respectively. Furthermore, the total pore volumes for these samples are 0.5663 cm³ g^{−1} and 0.3856 cm³ g^{−1}, respectively. The pore size distribution of both MIL-125(Ti)-NH₂ and MIL-125(Ti)-N(CH₂PO₃H₂)₂ based on the BJH method are shown in (Fig. 8b). As shown in this figure the pore size of both samples are less than 2 nm revealing the presence of micropores in the samples.

In another investigation, thermal gravimetric (TG) and derivative thermogravimetry (DTG) were applied for thermal and behavioral stability of MIL-125(Ti)-N(CH₂PO₃H₂)₂ (Fig. 9).

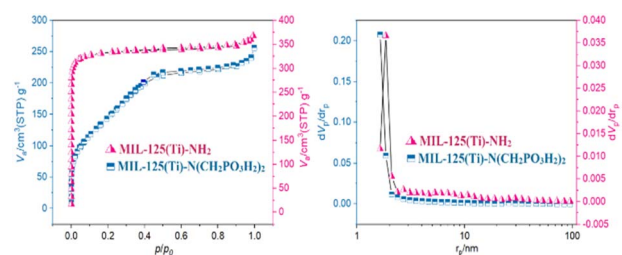


Fig. 8 N₂ absorption–desorption isotherm and pore size distribution based on BJH method for MIL-125(Ti)-NH₂ (▲) and MIL-125(Ti)-N(CH₂PO₃H₂)₂ (■) as a porous catalyst.

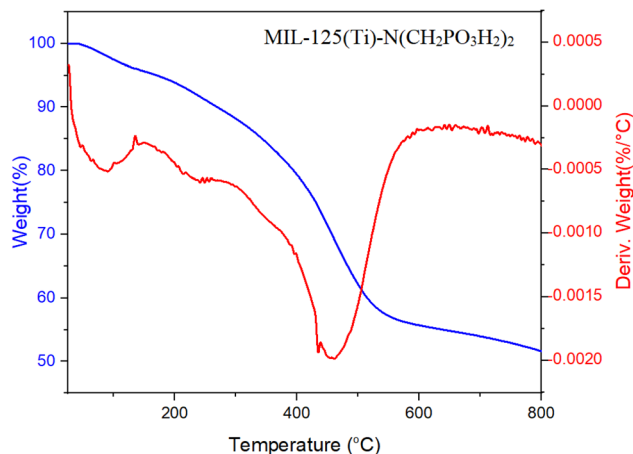
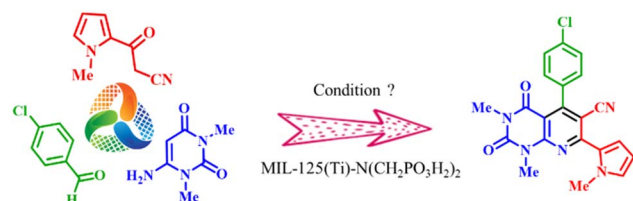


Fig. 9 TG and DTG analysis of MIL-125(Ti)-N(CH₂PO₃H₂)₂ as a porous catalyst.

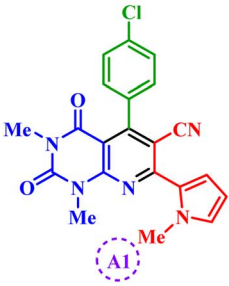
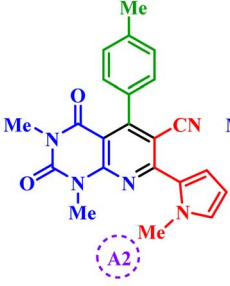
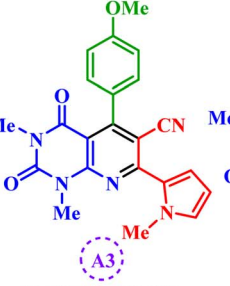
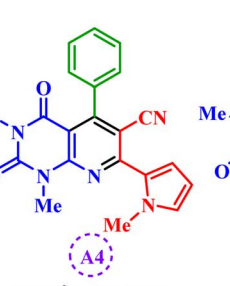

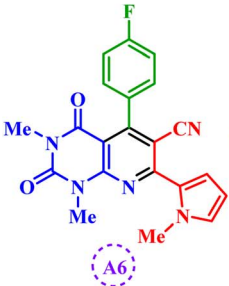
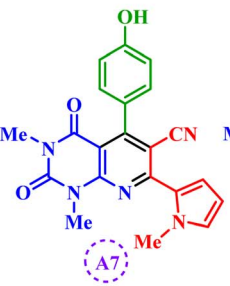
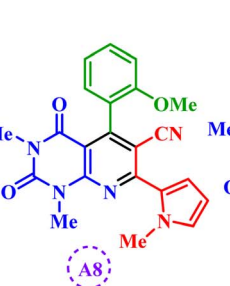
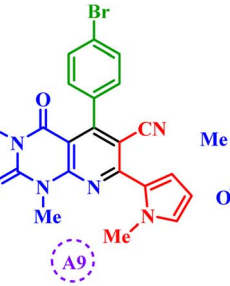

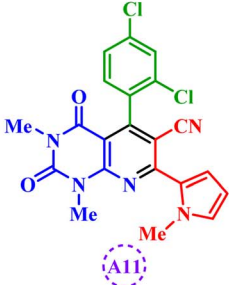
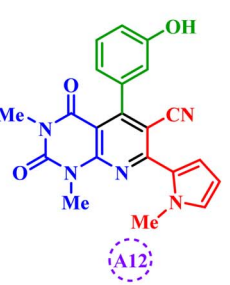
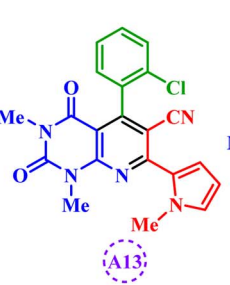
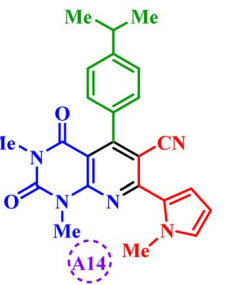
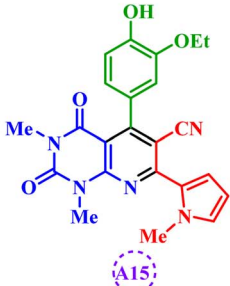
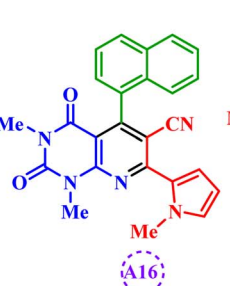
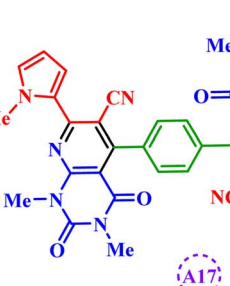
According to Fig. 9, the weight loss around 25–100 °C is related to the evaporation and removal of solvents (organic and H₂O) in the synthesis of the catalyst. Also, the weight loss around 450 °C is suggested to be the decomposition and breaking of organic sections (bond of N–C–PO₃H₂) of metal–organic frameworks (MOFs). Therefore, obtained data show thermal stability excellent of MIL-125(Ti)-N(CH₂PO₃H₂)₂, which can be used as a porous catalyst for organic reaction.

Table 1 Effect of different amounts of catalysts, temperature and solvent (5 mL) in the synthesis of novel tetrahydropyrido[2,3-d]pyrimidines



Entry	Solvent	Catalyst (mg)	Temp. (°C)	Time (min)	Yield (%)
1	—	10	110	40	83
2	—	10	100	35	90
3	—	10	90	50	82
4	—	10	50	100	30
5	—	10	25	120	—
6	—	20	100	35	85
7	—	15	100	40	70
8	—	5	100	100	55
9	—	—	100	180	—
10	H ₂ O	10	Reflux	180	—
11	EtOH	10	Reflux	100	70
12	CH ₂ Cl ₂	10	Reflux	180	—
13	CHCl ₃	10	Reflux	100	—
14	EtOAc	10	Reflux	120	10
15	DMF	10	100	150	72
16	MeOH	10	Reflux	120	45
17	CH ₃ CN	10	Reflux	120	55

Table 2 Synthesis of tetrahydropyrido[2,3-*d*]pyrimidine derivatives using MIL-125(Ti)-N(CH₂PO₃H₂)₂ as a porous catalyst^a

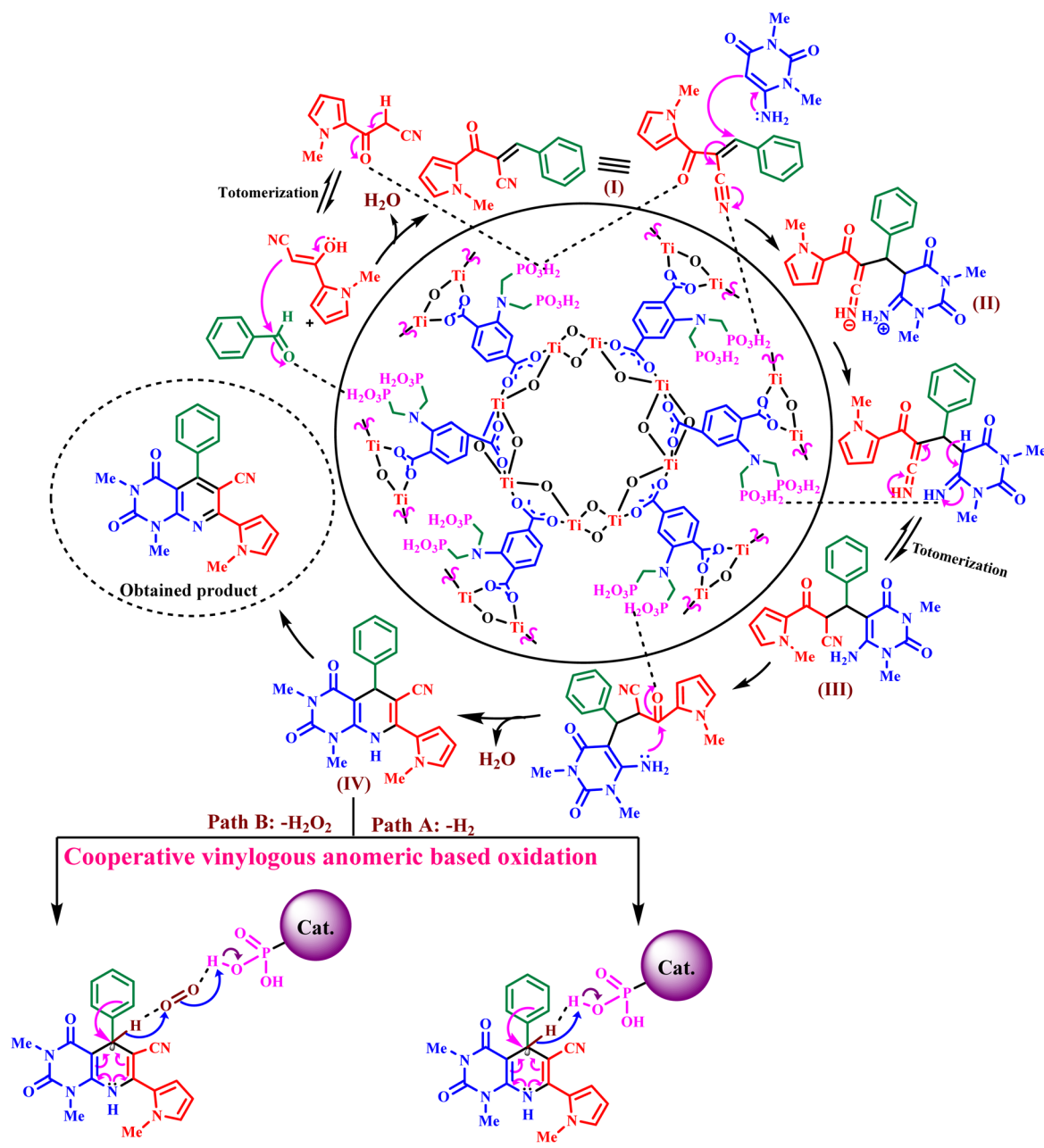
				
M.P (°C):248-250 Yield (%):90 Time (min.): 35	M.P (°C): 228-230 Yield (%): 85 Time (min.): 35	M.P (°C): 230-233 Yield (%): 79 Time (min.): 60	M.P (°C): 228-230 Yield (%): 85 Time (min.): 40	M.P (°C): 180-182 Yield (%): 70 Time (min.): 60
				
M.P (°C): 289-290 Yield (%): 80 Time (min.): 45	M.P (°C): >300 Yield (%): 89 Time (min.): 30	M.P (°C): 205-208 Yield (%): 83 Time (min.): 35	M.P (°C): 266-268 Yield (%): 85 Time (min.): 50	M.P (°C): 233-235 Yield (%): 80 Time (min.): 45
				
M.P (°C): 210-213 Yield (%): 90 Time (min.): 40	M.P (°C): 156-158 Yield (%): 78 Time (min.): 60	M.P (°C): >300 Yield (%): 70 Time (min.): 45	M.P (°C): 190-192 Yield (%): 88 Time (min.): 60	
				
M.P (°C): 246-248 Yield (%): 90 Time (min.): 35	M.P (°C): 212-214 Yield (%): 79 Time (min.): 60	M.P (°C): >300 Yield (%): 85 Time (min.): 50		

^a Reaction conditions: a mixture of aryl aldehydes (1 mmol), 6-amino-1,3-dimethylpyrimidine-2,4(1*H*,3*H*)-dione (1 mmol, 0.155 g), 3-(1-methyl-1*H*-pyrrol-2-yl)-3-oxopropanenitrile (1 mmol, 0.148 g) and MIL-125(Ti)-N(CH₂PO₃H₂)₂ (10 mg) under solvent-free condition at 100 °C.

After the design, preparation, and characterization of MIL-125(Ti)-N(CH₂PO₃H₂)₂ as an acidic catalyst, the catalytic behavior of novel porous metal-organic framework was examined in the synthesis of tetrahydropyrido[2,3-*d*]pyrimidine derivatives *via* a cooperative vinylogous anomeric based oxidation. The above-mentioned catalyst was achieved one pot reaction of 4-chloro benzaldehyde (1 mmol, 0.140 g), 6-amino-1,3-dimethylpyrimidine-2,4(1*H*,3*H*)-dione (1 mmol, 0.155 g) and 3-(1-methyl-1*H*-pyrrol-2-yl)-3-oxopropanenitrile (1 mmol, 0.148 g) as a model reaction. The optimized reaction data is listed in Table 1. In this table, the model reaction was studied by using several solvents such as H₂O, EtOH, CH₂Cl₂, CHCl₃, EtOAc,

DMF, MeOH and CH₃CN (10 mL) in the presence of 10 mg of MIL-125(Ti)-N(CH₂PO₃H₂)₂ under reflux condition (Table 1, entries 10–17). Also, the model reaction was studied by using different amounts of catalysts (Table 1, entry 6–9) and temperatures (Table 1, entry 1–5). Considering the data reaction obtained (yield and time), the best results for the preparation of tetrahydropyrido[2,3-*d*]pyrimidines were achieved under solvent-free conditions at 100 °C and in the presence of MIL-125(Ti)-N(CH₂PO₃H₂)₂ (10 mg) as a porous catalyst (Table 1, entry 2).

After optimizing the reaction conditions for the preparation of novel tetrahydropyrido[2,3-*d*]pyrimidines, the performance



Scheme 4 Plausible mechanism in the synthesis of tetrahydropyrido[2,3-*d*]pyrimidine derivatives.

and application of MIL-125(Ti)-N(CH₂PO₃H₂)₂ as a porous metal-organic framework catalyst was further evaluated. The obtained results are summarized in Table 2. According to this table, the synthesis of tetrahydropyrido[2,3-*d*]pyrimidines were carried out under optimal conditions by using various aromatic aldehydes, including electron-bearing groups, electron-accepting groups, and halogen groups. The obtained results show that the yield of the products is high and the time of conducting the experiments is short. These results show the suitable catalytic performance of MIL-125(Ti)-N(CH₂PO₃H₂)₂, which can be extended to synthesis other organic compounds.

In the suggested mechanism, the aldehyde is activated by the catalyst and reacts with 3-(1-methyl-1*H*-pyrrol-2-yl)-3-oxopropanenitrile, which has been converted to its tautomeric form by the catalyst, and intermediate (I) is created. Intermediate (I) as a Michael acceptor is activated by the catalyst and is attacked by the uracil nucleophile. The intermediate (II) produced in this step is converted to intermediate (III) by proton transfer and tautomerization. Intermediate (III) is converted into intermediate (IV) by performing an intramolecular cyclization reaction and losing another H₂O molecule. In the next step, intermediate (III) is converted into intermediate (IV) by performing an intramolecular cyclization reaction and losing another H₂O molecule. In the next step, intermediate (IV) *via* “a cooperative geminal-vinylogous anomeric affect” through simultaneously electron sharing from phenyl group and lone pair electrons of N atoms through C=C bonds into the anti-bonding of C-H bond causes the releasing of hydride which has been named “cooperative geminal-vinylogous anomeric based oxidation” mechanism in the presence and absence of oxygen pathways A and B in Scheme 4 (in the main manuscript text) respectively. During this mechanism, hydrogen molecule (-H₂) or hydrogen peroxide molecule (-H₂O₂) whose oxygen is supplied from the air is released. The above-mentioned concept has been reviewed comprehensively.^{34,43} To investigate the activation of aldehyde by catalyst, *p*-chloro benzaldehyde was

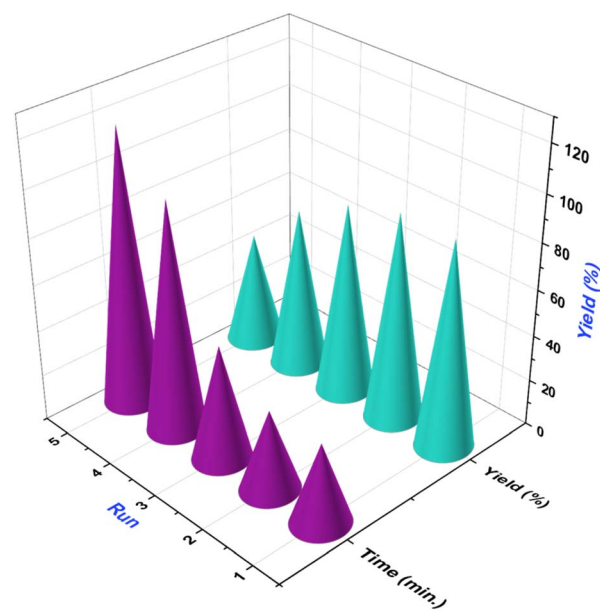


Fig. 10 Reusability of MIL-53(Al)-N(CH₂PO₃H₂)₂ for the synthesis of novel tetrahydropyrido[2,3-*d*]pyrimidines.

activated with MIL-125(Ti) and MIL-125(Ti)-N(CH₂PO₃H₂)₂ at room temperature. Then the FT-IR spectra of the reaction mixtures were studied. The absorption band of C=O of the *p*-chloro benzaldehyde at 1692 cm⁻¹ was changed to 1694 and 1702 cm⁻¹ in the presence of MIL-125(Ti) and MIL-125(Ti)-N(CH₂PO₃H₂)₂ respectively (Fig. S1, see in ESI†).

To evaluate reactivity of catalyst, the reaction of 4-chloro benzaldehyde (1 mmol, 0.140 g), 6-amino-1,3-dimethylpyrimidine-2,4(1*H*,3*H*)-dione (1 mmol, 0.155 g) and 3-(1-methyl-1*H*-pyrrol-2-yl)-3-oxopropanenitrile (1 mmol, 0.148 g) as a model reaction was evaluated by MIL-125(Ti)-N(CH₂PO₃H₂)₂ and other catalyst such as organic, inorganic and solid acids (Table 3). As shown in Table 3, the MIL-125(Ti)-N(CH₂PO₃H₂)₂ is the best

Table 3 Evaluation of various catalyst for the synthesis of novel tetrahydropyrido[2,3-*d*]pyrimidines in comparison with MIL-125(Ti)-N(CH₂PO₃H₂)₂

Entry	Catalyst ^a	Amount of catalyst	Time (min)	Yield (%)
1	<i>p</i> -TSA	10 mol%	100	20
2	NaOH	10 mol%	120	30
3	Et ₃ N	10 mol%	120	25
4	GTMPA ²¹	10 mol%	100	43
5	MIL-53(Al)-N(CH ₂ PO ₃ H ₂) ₂ (ref. 18 and 19)	10 mg	60	75
6	CQDs-N(CH ₂ PO ₃ H ₂) ₂ (ref. 24)	10 mg	80	60
7	APVPB ⁴⁴	10 mg	120	35
8	GTBSA ⁴⁵	10 mol%	180	65
9	Fe ₃ O ₄ @Co(BDC)-NH ₂ (ref. 46)	10 mg	110	53
10	[PVI-SO ₃ H]FeCl ₄ (ref. 47)	10 mg	100	40
11	SSA ^{48,49}	10 mg	80	35
12	MIL-125(Ti)-NH ₂	10 mg	120	52
13	PO ₃ H ₃	10 mol%	90	40
14	MIL-125(Ti)-N(CH₂PO₃H₂)₂ this work	10 mg	35	90

^a The reaction of 4-chloro benzaldehyde (1 mmol, 0.140 g), 6-amino-1,3-dimethylpyrimidine-2,4(1*H*,3*H*)-dione (1 mmol, 0.155 g) and 3-(1-methyl-1*H*-pyrrol-2-yl)-3-oxopropanenitrile (1 mmol, 0.148 g) at 100 °C under solvent-free condition.

performance for the synthesis of tetrahydropyrido[2,3-*d*]pyrimidines. Also, the recyclability of MIL-125(Ti)-N(CH₂PO₃H₂)₂ was checked out in the model reaction. The results show that the MIL-125(Ti)-N(CH₂PO₃H₂)₂ has the potential to be recycled and reused up to 4 times without significant decreasing its catalytic activity (Fig. 10).

4 Conclusions

In this paper, we reported new metal–organic frameworks (MOFs) containing phosphorous acid tags namely MIL-125(Ti)-N(CH₂PO₃H₂)₂ as a porous catalyst. This mesoporous catalyst was characterized by several techniques such as FT-IR, EDX, XRD, SEM, N₂ adsorption–desorption isotherms, BJH/BJH and TG/DTG analysis. Then, its catalytic application in the synthesis of new series of tetrahydropyrido[2,3-*d*]pyrimidines via a cooperative vinylogous anomeric-based oxidation mechanism. Easy separation of catalyst from mixture reaction, clean profile of reaction and widespread new synthesis of biologically active with good to excellent yields are most important of described work.

Conflicts of interest

The authors declare no competing financial interests.

Acknowledgements

We thank the Bu-Ali Sina University and Iran National Science Foundation (INSF) (Grant Number: 4012835) for financial support.

References

- 1 A. R. Millward and O. M. Yaghi, *J. Am. Chem. Soc.*, 2005, **127**, 17998–17999.
- 2 (a) H. Sepehrmansourie, *Iran. J. Catal.*, 2021, **11**, 207–215; (b) H. Sepehrmansourie, M. Zarei, M. A. Zolfigol, S. Kalhor and H. Shi, *Mol. Catal.*, 2022, **531**, 112634.
- 3 (a) M. J. Kalmutzki, C. S. Diercks and O. M. Yaghi, *Adv. Mater.*, 2018, **30**, 1704304; (b) H. Sepehrmansourie, H. Alamgholiloo, N. Noroozi Pesyan and M. A. Zolfigol, *Appl. Catal., B*, 2022, **321**, 122082.
- 4 J. Lee, O. K. Farha, J. Roberts, K. A. Scheidt, S. T. Nguyen and J. T. Hupp, *Chem. Soc. Rev.*, 2009, **38**, 1450–1459.
- 5 L. Liu, Y. Zhou, S. Liu and M. Xu, *ChemElectroChem*, 2018, **5**, 6–19.
- 6 K. Huang, B. Wang, S. Guo and K. Li, *Angew. Chem.*, 2018, **57**, 13892–13896.
- 7 F. Ghamari, D. Raoufi, S. Alizadeh, J. Arjomandi and D. Nematollahi, *J. Mater. Chem. A*, 2021, **9**, 15381–15393.
- 8 X. Zhang, T. Kitao, D. Piga, R. Hongu, S. Bracco, A. Comotti, P. Sozzani and T. Uemura, *Chem. Sci.*, 2020, **11**, 10844–10849.
- 9 N. Ottman, L. Ruokolainen, A. Suomalainen, H. Sinkko, P. Karisola, J. Lehtimäki, M. Lehto, I. Hanski, H. Alenius and N. Fyhrquist, *J. Allergy Clin. Immunol.*, 2019, **143**, 1198–1206.
- 10 (a) X. Kong, H. Deng, F. Yan, J. Kim, J. A. Swisher, B. Smit, O. M. Yaghi and J. A. Reimer, *Science*, 2013, **341**, 882–885; (b) H. Sepehrmansourie, M. Zarei, M. A. Zolfigol, S. Babae, S. Azizian and S. Rostamnia, *Sci. Rep.*, 2022, **12**, 14145; (c) E. Tavakoli, H. Sepehrmansourie, M. Zarei, M. A. Zolfigol, A. Khazaei and M. Hosseinfard, *New J. Chem.*, 2022, **46**, 19054–19061.
- 11 F. Wang, C. Wang, Z. Yu, K. Xu, X. Li and Y. Fu, *Polyhedron*, 2016, **105**, 49–55.
- 12 S. L. Griffin and N. R. Champness, *Coord. Chem. Rev.*, 2020, **414**, 213295.
- 13 D. Banerjee and J. B. Parise, *Cryst. Growth Des.*, 2011, **11**, 4704–4720.
- 14 H. L. Nguyen, *J. Phys.: Energy*, 2021, **3**, 021003.
- 15 A. P. Smalley, D. G. Reid, J. C. Tan and G. O. Lloyd, *CrystEngComm*, 2013, **15**, 9368–9371.
- 16 A. M. Naseri, M. Zarei, S. Alizadeh, S. Babae, M. A. Zolfigol, D. Nematollahi, J. Arjomandi and H. Shi, *Sci. Rep.*, 2021, **11**, 16817.
- 17 H. Sepehrmansouri, M. Zarei, M. A. Zolfigol, A. R. Moosavi-Zare, S. Rostamnia and S. Moradi, *Mol. Catal.*, 2020, **481**, 110303.
- 18 S. Kalhor, M. Zarei, M. A. Zolfigol, H. Sepehrmansourie, D. Nematollahi, S. Alizadeh, H. Shi and J. Arjomandi, *Sci. Rep.*, 2021, **11**, 19370.
- 19 S. Babae, M. Zarei, H. Sepehrmansourie, M. A. Zolfigol and S. Rostamnia, *ACS Omega*, 2020, **5**, 6240–6249.
- 20 F. Jalili, M. Zarei, M. A. Zolfigol and A. Khazaei, *RSC Adv.*, 2022, **12**, 9058–9068.
- 21 (a) S. Moradi, M. A. Zolfigol, M. Zarei, D. A. Alonso and A. Khoshnood, *ChemistrySelect*, 2018, **3**, 3042–3047; (b) B. Danishyar, H. Sepehrmansourie, M. Zarei, M. A. Zolfigol, M. A. As' Habi and Y. Gu, *Polycyclic Aromat. Compd.*, 2022, 1–21.
- 22 F. Jalili, M. Zarei, M. A. Zolfigol, S. Rostamnia and A. R. Moosavi-Zare, *Microporous Mesoporous Mater.*, 2020, **294**, 109865.
- 23 J. Afsar, M. A. Zolfigol, A. Khazaei, M. Zarei, Y. Gu, D. A. Alonso and A. Khoshnood, *Mol. Catal.*, 2020, **482**, 110666.
- 24 M. Mohammadi Rasooll, M. Zarei, M. A. Zolfigol, H. Sepehrmansourie, A. Omidi, M. Hasani and Y. Gu, *RSC Adv.*, 2021, **11**, 25995–26007.
- 25 G. Jubete, R. Puig de la Bellacasa, R. Estrada-Tejedor, J. Teixidó and J. I. Borrell, *Molecules*, 2019, **24**, 4161.
- 26 M. N. Yousif, A. R. El-Gazzar and M. M. El-Enany, *Mini-Rev. Org. Chem.*, 2021, **18**, 43–54.
- 27 C. Kurumurthy, P. S. Rao, P. S. Rao, B. Narsaiah, L. Velatooru, R. Pamanji and J. V. Rao, *Eur. J. Med. Chem.*, 2011, **46**, 3462–3468.
- 28 A. Bazgir, M. M. Khanaposhtani, R. Ghahremanzadeh and A. A. Soorki, *C. R. Chim.*, 2009, **12**, 1287–1295.
- 29 V. Cody, J. Pace, O. A. Namjoshi and A. Gangjee, *Acta Crystallogr., Sect. F: Struct. Biol. Commun.*, 2015, **71**, 799–803.
- 30 A. Gangjee, O. A. Namjoshi, S. Raghavan, S. F. Queener, R. L. Kisliuk and V. Cody, *J. Med. Chem.*, 2013, **56**, 4422–4441.

- 31 Z. Toobaei, R. Yousefi, F. Panahi, S. Shahidpour, M. Nourisefat, M. M. Doroodmand and A. Khalafi-Nezhad, *Carbohydr. Res.*, 2015, **411**, 22–32.
- 32 (a) E. Juaristi and G. Cuevas, *Tetrahedron*, 1992, **48**, 5019–5087; (b) V. Alabugin, L. Kuhn, N. V. Krivoshchapov, P. Mehaffy and M. G. Medvedev, *Chem. Soc. Rev.*, 2021, **50**, 10212.
- 33 (a) I. V. Alabugin, *Stereoelectronic effects: a bridge between structure and reactivity*, John Wiley & Sons, 2016; (b) I. V. Alabugin, L. Kuhn, M. G. Medvedev, N. V. Krivoshchapov, V. A. Vil, I. A. Yaremenko, P. Mehaffy, M. Yarie, A. O. Terent'ev and M. A. Zolfigol, *Chem. Soc. Rev.*, 2021, **50**, 10253.
- 34 M. Yarie, *Iran. J. Catal.*, 2017, **7**, 85–88.
- 35 C. B. Bai, N. X. Wang, Y. Xing and X. W. Lan, *Synlett*, 2017, **28**, 402–414.
- 36 T. He, R. Shi, Y. Gong, G. Jiang, M. Liu, S. Qian and Z. Wang, *Synlett*, 2016, **27**, 1864–1869.
- 37 G. Hamasaka, H. Tsuji and Y. Uozumi, *Synlett*, 2015, **26**, 2037–2041.
- 38 S. N. Kim, J. Kim, H. Y. Kim, H. Y. Cho and W. S. Ahn, *Catal. Today*, 2013, **204**, 85–93.
- 39 H. M. Al-Matar, A. Y. Adam, K. D. Khalil and M. H. Elnagdi, *Arkivoc*, 2012, **6**, 1–15.
- 40 Y. Zhao, W. Cai, J. Chen, Y. Miao and Y. Bu, *Front. Chem.*, 2019, **7**, 789.
- 41 R. Zhang, G. Li and Y. Zhang, *Photochem. Photobiol. Sci.*, 2017, **16**, 996–1002.
- 42 M. Nasalevich, R. Becker, E. Ramos-Fernandez, S. Castellanos, S. Veber, M. Fedin, F. Kapteijn, J. Reek, J. Van Der Vlugt and J. Gascon, *Energy Environ. Sci.*, 2015, **8**, 364–375.
- 43 M. Yarie, *Iran. J. Catal.*, 2020, **10**, 79–83.
- 44 E. Noroozizadeh, A. R. Moosavi-Zare, M. A. Zolfigol, M. Zarei, R. Karamian, M. Asadbegy, S. Yari and S. H. Moazzami Farida, *J. Iran. Chem. Soc.*, 2018, **15**, 471–481.
- 45 M. Zarei, H. Sepehrmansourie, M. A. Zolfigol, R. Karamian and S. H. Moazzami Farida, *New J. Chem.*, 2018, **42**, 14308–14317.
- 46 H. Sepehrmansourie, M. Zarei, M. A. Zolfigol, S. Babaee and S. Rostamnia, *Sci. Rep.*, 2021, **11**, 5279.
- 47 H. Sepehrmansourie, M. Zarei, R. Taghavi and M. A. Zolfigol, *ACS Omega*, 2019, **4**, 17379–17392.
- 48 M. A. Zolfigol, *Tetrahedron*, 2001, **57**, 9509–9511.
- 49 H. Sepehrmansourie, *Iran. J. Catal.*, 2020, **10**, 175–179.